Electronic Raman scattering in graphite and single-layer and few-layer graphene

Yu. S. Ponosov,[1,*] A. V. Ushakov,[1] and S. V. Streltsov[1,2]

[1]*M. N. Miheev Institute of Metal Physics UB RAS, 620990, S. Kovalevskaya Str. 18, Ekaterinburg, Russia*
[2]*Ural Federal University, 620002, Mira Str. 19, Ekaterinburg, Russia*

We investigated polarization-resolved electronic Raman scattering in different graphitic structures, including bulk graphite and single-layer and few-layer graphene. For all investigated samples, the broad continua of interband electronic transitions were detected at an energy ∼0.35 eV, while they were expected to be at ∼6 eV [Phys. Rev. B **88**, 085416 (2013)]. The symmetry of the observed excitations corresponds to the A_{2g} irreducible representation. A quasilinear behavior of the Raman response is observed at low energies in all cases at room temperature, in agreement with performed tight-binding calculations. High-energy features at ∼0.8 eV are detected in the spectra of graphite and few-layer graphene. They are attributed to interband transitions in the vicinity of the K point, which involve electronic bands split by interlayer interaction. The effects of the substrate type, defect amount, and doping on the continuum line shape and symmetry are discovered. The silent layer-breathing mode is observed in a single-layer graphene. The results evidence that the electronic light scattering in graphitic structures without an external magnetic field is a powerful tool, which provides a variety of data on the structure and symmetry of low-energy electronic excitations.

I. INTRODUCTION

For the last 10 years since two-dimensional crystals of graphene were produced [1], intense experimental and theoretical studies of graphene's electronic properties have been performed. Its low-energy electronic structure has been investigated with angle-resolved photoemission spectroscopy (ARPES) and optical absorption [2–8] in single-layer (SLG) and multilayered (MLG) graphene structures including three-dimensional (3D) graphite [9]. Being the most powerful tool for the characterization of graphitic structures and study of their phonon spectra [10,11], Raman spectroscopy recently has also been applied to study electronic excitations. Electronic light scattering is known to be a method of investigation of long-wave charge- and spin-density fluctuations due to particle-hole excitations, and it has been widely used to study metallic and semiconductor systems [12–15].

Due to the crystal structure of graphitic systems having two atoms in a honeycomb layer, the band structure of an SLG contains two degenerate linear 2D bands in the valence and conduction zones, touching each other in the Dirac points K and K' of the hexagonal Brillouin zone (BZ). In the case of bilayer graphene (BLG), the appearance of the second π^* band leads to a parabolic dispersion of touching low-frequency bands near the K point and second pair of split bands. The electronic structure of 3D graphite is characterized by a BLG-like dispersion (massive fermions) in the K points and linear dispersion (massless fermions) in the H points of the BZ. Thus the main source of electronic Raman scattering (ERS) in graphitic systems in the clean limit can be direct interband electronic transitions with small wave vectors $q \sim 10^5$–10^5 cm^{-1}, contrary to normal metals where intraband transitions prevail.

A theory of inelastic light scattering by electronic excitations in SLG and BLG, both with and without an external magnetic field, has been presented in [16–20]. Calculated in [16,17], the Raman spectra of graphene in normal and superconducting states show a linearly increasing intensity with a maximum near 6 eV in the clean limit for the case when the Fermi level E_F is in the charge neutrality point. In doped graphene, ERS is forbidden up to the particle-hole threshold frequency $\omega = 2|E_F|$. In the presence of impurities or defects, the intraband scattering within this gap becomes possible.

The authors of [18–20] presented a detailed theory of the low-energy ERS both in SLG and BLG. Although the frequency behavior of the spectrum for SLG at zero magnetic field was found to be similar to that found in [16,17], three important items have been addressed. First, it was shown that the symmetry of electronic excitations should be of the A_2 type for the C_{6v} layer point group (or A_{2g} type for the D_{6h} point group), which describes a pseudo-spin-flip process. Second, it was found that the mechanism of scattering is dominated by the **A*****p** term in the Hamiltonian describing the interaction of the electron momentum **p** with the vector potential **A** of the electromagnetic field via virtual intermediate electronic states. Finally, the intensity of the intraband contribution was estimated to be negligible compared to the interband contribution. It was shown also that the low-frequency behavior of the ERS spectrum should be energy independent in BLG, contrary to the linear increase of the spectral intensity in SLG.

Some of these features have been confirmed in Raman measurements [21–26] with a magnetic field, where symmetries and field dependencies of magnetoexcitons and magnetophonon resonance between the E_{2g} phonon (G mode) and inter-Landau level electronic excitations have been established. However, ERS without a magnetic field has not been investigated in great detail so far. The published spectra were measured in the limited energy range (only up to 160 cm^{-1}) and did not provide information about the ERS line shape in a broad frequency scale [26].

This work presents polarization-resolved measurements of ERS at zero magnetic field over a wide energy range of up to 1 eV for graphite, SLG, and few-layer graphene.

---

*ponosov@imp.uran.ru

In all investigated structures, distinct continua of chiral electronic excitations, which are accompanied by transitions involving high-energy split bands, were observed. The symmetries and line shapes of these discovered excitations were found to be sensitive to the doping level, defect amount, and effects of interaction with a substrate. The frequency dependencies of the experimental ERS spectra were well described by calculations based on the tight-binding band structure.

II. EXPERIMENT

The measurements were carried out on fresh surfaces of highly oriented pyrolitic graphite (HOPG) having the *c*-axis misorientation of ∼0.5°. Graphene layers were prepared by mechanical cleavage from this graphite crystal and transferred onto a silicon substrate covered with a 300-nm silicon-oxide layer or onto an electropolished cobalt single-crystal plate. To identify SLG and few-layer graphene, line shape and width of the phonon overton 2D line were measured using two laser energies.

Raman spectra were excited with the 532-nm (2.33-eV) and 633-nm (1.96-eV) laser lines with an average power of 3 mW focused onto the sample by a 50× objective lens with a numerical aperture of 0.55. The scattered light was collected by a Renishaw microspectrometer RM1000 equipped with a thermocooled CCD detector. The edge filters used provided a cutoff energy of ∼50 cm^{-1} from the laser line. The spectral resolution was about 2.5 cm^{-1}. For temperature-dependent measurements, the graphite sample under study was placed into an optical microscopy cryostat (Microstat He2, Oxford).

Polarization measurements were carried out both with linear and circular polarizations to identify the A_{2g} antisymmetric tensor. A quarter-wave plate placed before an objective lens was used to circularly polarize the excitation beam and the collected signal. A set of half-wave plate and linear polarizer was then used to provide a required scattering geometry. For the graphite space group *P* 63/*mmc* there are four Raman active symmetries: $A_{1g}+A_{2g}+E_{1g}+E_{2g}$. With parallel linear polarizations of the incident and scattered radiation in the layer (XX or YY), the A_{1g} and E_{2g} tensors can be measured, whereas the cross-polarization geometries (XY, YX) contain the A_{2g} and E_{2g} symmetries. The A_{1g} and A_{2g} symmetries can be observed using the cocircular polarization geometries ($\sigma^+\sigma^+$, $\sigma^-\sigma^-$), while the cross-circular ($\sigma^+\sigma^-$, $\sigma^-\sigma^+$) geometries isolate the E_{2g} symmetry.

The intensity of the ERS spectra in graphitic structures is very weak, being by 20–50 times less than the intensity of the *G* mode, so such spectra are strongly disturbed, especially for thin layers, by a contribution from the substrate whose spectrum should be subtracted from the measured spectrum. Yet it is difficult to obtain a real ERS spectrum in the case of the Si/SiO$_2$ substrate, especially for the parallel polarization geometry, because a subtracting of intense substrate spectrum results in a noise enhancement and an appearance of outliers (phonon remnants) in the low-frequency range of the final spectrum. Using the cobalt substrate substantially reduces such a problem because the Co substrate itself gives a rather weak and featureless spectrum, which accounts for all elastic and inelastic light-scattering contributions along the spectrometer

beam path (from lens, filters, etc.). In the case of graphite the spectra measured without the sample were subtracted.

Since the measurements were carried out in a wide energy range, measured spectra after the above-mentioned subtractions were corrected for the spectral response of the spectrometer, and transmission and absorption coefficients in the frequency range of the scattered light as well. All represented spectra then were divided by $[n(\omega,T)+1]$, where $n(\omega,T)$ is the Bose-Einstein factor.

III. CALCULATIONS

In order to understand the frequency behavior of ERS in all studied structures at different temperatures and to separate contributions from interband transitions near the *K* and the *H* points of the BZ in graphite, we performed calculations of the electronic structure and ERS spectra. We used the approach of Ref. [27], where the tight-binding Hamiltonian describing the band structure near the Fermi energy was constructed for a general number of graphene layers. Values of the tight-binding parameters used for different numbers of graphene layers were taken from [28]. The frequency dependence of the Raman cross section for the interband scattering with the momentum transfer $q \sim 0$ is determined by

$$I_{\alpha,\beta}^{\text{inter}}(\omega) \propto \frac{1}{1 - \exp\frac{-\hbar\omega}{kT}} |\gamma_{\alpha,\beta}(p)|^2 \cdot \sum_{m_c,n_v} \int d^3p$$
$$\times [f_p(\epsilon_c) - f_p(\epsilon_v)] \cdot \left(\frac{1}{\omega + (\epsilon_c - \epsilon_v) + i\delta} \right.$$
$$\left. - \frac{1}{\omega - (\epsilon_c - \epsilon_v) + i\delta} \right), \quad (1)$$

where $\gamma_{\alpha,\beta}(p)$ is the matrix element of electron-photon interaction, $f_p(\epsilon_{c/v})$ are the Fermi functions of electronic states in the conduction (m_c) and valence (n_v) bands, and δ is the electron relaxation rate. The integration was performed over the whole BZ; in order to isolate transitions from the *H* and *K* points, two dimensional integration was performed in the vicinity of these points. The matrix elements of the electron-photon interaction were taken constant because no energy dependence of them was found in [18]. We also proposed the clean limit regime using the small damping of the electronic states $\delta \sim$ 10 cm^{-1} in our simulations.

IV. RESULTS AND DISCUSSION

An intense Raman scattering by main phonons in graphitic structures (the G mode and the 2D phonon overtone) is superimposed on a weak background whose line shape and symmetry have not been investigated in detail so far. In order to confirm that this background is due to the Raman effect, the measurements were made using two excitation energies.

In Figs. 1 and 2, the polarized graphite spectra excited with the 532-nm (2.33-eV) and 633-nm (1.96-eV) lasers are shown. In both cases, broad peaks are observed in the range of 3000 cm^{-1} (∼0.35 eV), indicating that the observed scattering is really the Raman effect. The limited energy range and a strong decrease of our spectrometer sensitivity at high energies for the 633-nm excitation explain the line-shape differences at high frequencies. Yet, the main result is apparent: in
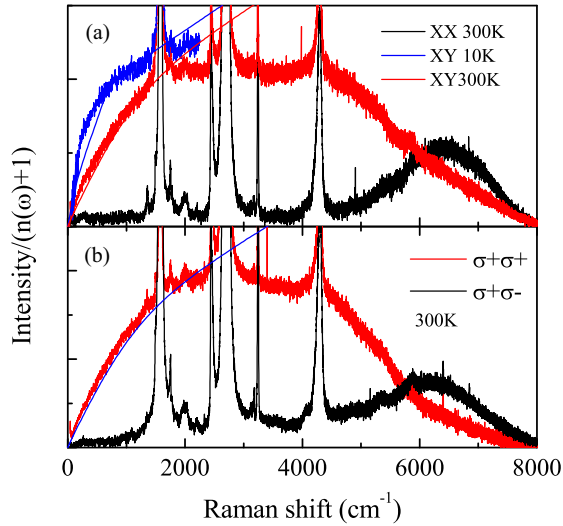
FIG. 1. (Color online) (a) Electronic Raman spectra of graphite, measured at 300 K and in low-energy range at 10 K with linear (a) and circular (b) polarizations using 532-nm excitation. Calculated spectra are shown by solid lines.

both cases, a quasilinear increase of Raman intensity takes place at low frequencies and the broad continua exist near $\sim$3000 cm^{-1} (0.35 eV). Such a behavior is observed both in geometries with the perpendicular (XY) linear polarizations probing the A_{2g} and E_{2g} symmetries [Figs. 1(a) and 2(a)], and with the cocircular polarization ($\sigma^+\sigma^+$) probing the A_{1g} and A_{2g} symmetries [Figs. 1(a) and 2(a)]. This unambiguously evidences the A_{2g} symmetry of the observed chiral electronic excitations predicted in [18–20]. The intensity of this scattering in the polarization geometries XX ($A_{1g}+E_{2g}$) or $\sigma^+\sigma^-$ (E_{2g}) is very weak, but the broad peak near 6500 cm^{-1} (0.8 eV) is
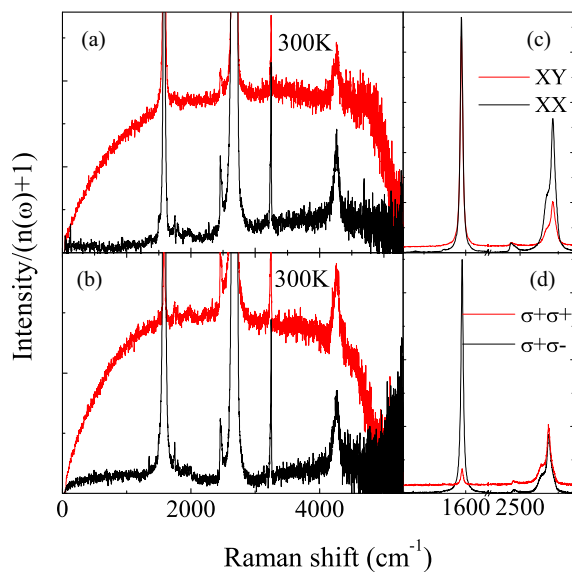
FIG. 2. (Color online) Electronic Raman spectra of graphite, measured with linear (a) and circular (b) polarizations using 633-nm excitation. Calculated spectra are shown by solid lines. Polarization-resolved phonon spectra are plotted in (c) and (d).

clearly seen in these geometries [Figs. 1(a) and 1(b)]. One may suggest that the symmetry of this band is E_{2g}, though it was not observed with the perpendicular (XY) linear polarizations probing the A_{2g} and E_{2g} symmetries.

The ARPES measurements in graphite [4] showed that the Dirac point at the H point of the BZ lies $\sim$50 meV above E_F. In this case, the spectrum of low-energy interband transitions should have a gap $\Delta E \sim 2E_F \sim$ (800 cm^{-1}) (100 meV). The low-frequency limit of our measurements was 50 cm^{-1}, but no gaplike intensity depletion was observed in the room-temperature measurements. To exclude an effect of a thermal smearing of spectra at low energies, the low-temperature measurements were carried out, which are shown in Fig. 1(a). The low-energy behavior is also linear, but the blocking of transitions lower 100 cm^{-1} is possible at 10 K.

The linear intensity growth found at lowest energies in the graphite spectra reminds one of the behavior predicted for ERS in SLG [16–18], which is determined by the linear increase of the density of states. But the electronic structure of graphite contains both the massless fermions at the H point and massive ones (having parabolic dispersion at low energies) at the K point of the BZ. The latter provide the constant spectral density of the interband excitations, so the low-temperature ERS arising from such transitions near the K point should be energy independent at low frequencies, as it has been proposed in [18–20]. To justify such a suggestion, separate spectra contributing to the total response in graphite were measured from the samples of SLG and BLG, as well as from a trilayer graphene.

Two samples of BLG were measured: the first was placed onto the cobalt and the second onto the Si/SiO$_2$ substrate. They were identified by the line shape and width of the 2D phonon band measured with the two excitation lines used [29] (Fig. S1 in Ref. [30]). A quasilinear intensity increase was observed in the XY spectrum of BLG on the Co substrate [Fig. 3(a)] at room temperature. The more detailed measurements in the low-energy range (see Fig. S2 in [30]) confirmed that this linear growth of the XY spectra starts from a finite intensity value. It may be due to the contribution of the excitations with the E_{2g} symmetry, which are also observed in the XX spectrum with an almost constant intensity at low energies (Fig. S2 in [30]). The energy position of the broad electronic continuum in the XY polarization geometry in the first BLG sample $\sim$2500 cm^{-1} (0.3 eV) is shifted to lower frequencies in comparison to the graphite spectrum. Only the weak featureless background is observed in the XX polarization geometry at these energies. In contrast, for the second BLG sample on the Si/SiO$_2$ substrate [Fig. 3(b)] similar continua of electronic excitations were detected near $\sim$3000 cm^{-1} (0.35 eV) in both polarization geometries that suggests the pseudospin symmetry breaking. The weak features at $\sim$6200 cm^{-1} (0.77 eV) were found in the parallel polarization geometry for both samples.

The band structure of trilayer graphene can be understood as a combination of the band structure of a SLG and the band structure of a BLG. As in the case of BLG, we studied two trilayer flakes transferred onto the cobalt and the Si/SiO$_2$ substrates. The line shapes of the 2D line and the energy positions of the combination modes in the range of 1700–2250 cm^{-1} were the same for both samples, indicating the ABA stacked graphene [29]. For the sample on the Co
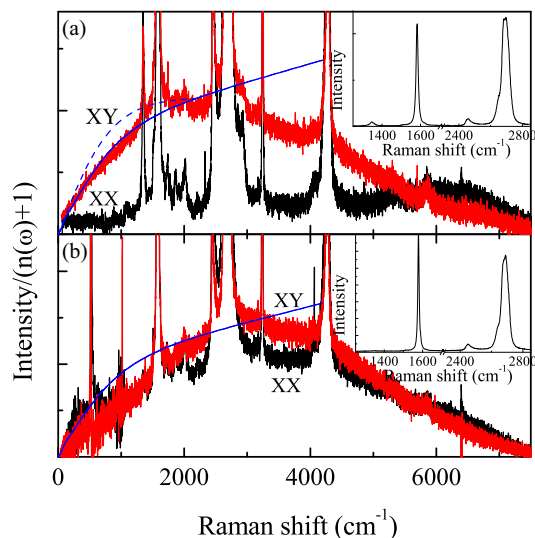
FIG. 3. (Color online) Electronic Raman spectra of two BLG flakes measured at 300 K with linear polarizations using 532-nm excitation: (a) Co substrate, (b) Si/SiO$_2$ substrate, (solid line) calculated with Eq. (1) spectrum, (dashed line) low-energy part of spectrum, calculated in parabolic band approximation. Insets show polarization-resolved phonon spectra of BLG samples.

substrate, the spectrum contains the intense continuum of chiral electronic excitations in the XY polarization geometry with the linear low-energy behavior and structureless low intense background having the high-frequency peak near 6200 cm^{-1} (0.77 eV) in the XX geometry [Fig. 4(a)]. As for BLG, the spectra of trilayer graphene on the Si/SiO$_2$ substrate have similar broad continua near 3000 cm^{-1} in both polarization geometries [Fig. 4(b)].

The Raman spectra measured from two SLG flakes are shown in Fig. 5. This experiment was done using graphene
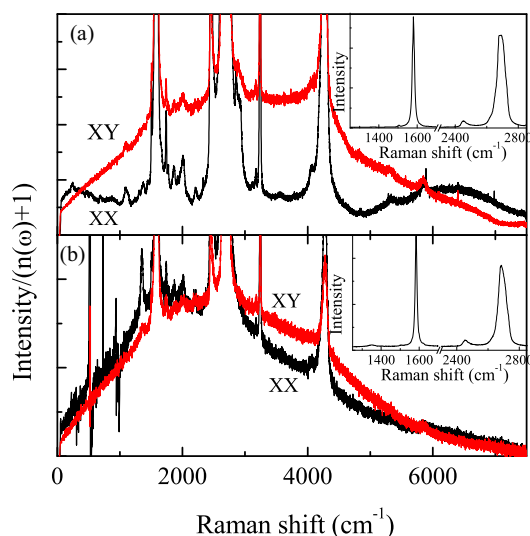
FIG. 4. (Color online) Electronic Raman spectra of trilayer graphene samples, measured at 300 K with linear polarizations using 532-nm excitation: (a) Co substrate, (b) Si/SiO$_2$ substrate. Insets show polarization-resolved phonon spectra of trilayer graphene samples.
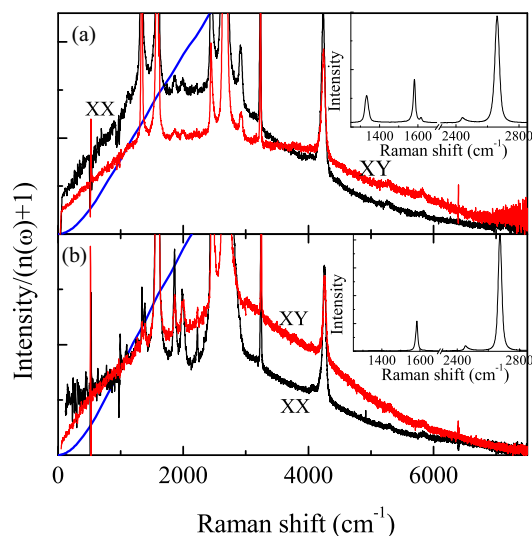
FIG. 5. (Color online) Electronic Raman spectra of two SLG samples on the Si/SiO$_2$ substrate measured at 300 K with linear polarizations using 532-nm excitation: (a) sample 1 with defects, (b) sample 2 with low defect density. Solid line presents the calculated spectrum. Insets show polarization-resolved phonon spectra of SLG samples.

transferred onto the Si/SiO$_2$ substrate, which provided a rather strong intensity compared to graphene on the cobalt substrate. Sample 1 had a ratio of the G/2D band intensities of ∼0.4, and the G phonon frequency and linewidth were 1582 cm^{-1} and ∼12 cm^{-1}, respectively. This indicated that the Fermi level was close to the Dirac point [31]. The strong intensity of the D line at 1332 cm^{-1} evidenced a large defect density in this sample [inset in Fig. 4(a)]. Sample 2 had a ratio of the G/2D band intensities of ∼0.25, and the G phonon frequency and linewidth were 1584 cm^{-1} and ∼12–13 cm^{-1}, respectively. In the spectrum of sample 2 the intensity of the D band was negligible, indicating a small number of defects. Again, as for graphite and few-layer graphene, we detected the electronic continua near 2500–3000 cm^{-1} (∼0.35 eV) in the perpendicular (XY) polarization geometry. The broad continua with somewhat lower energies were observed also in the parallel (XX) polarization geometry for both studied samples. We note also that in the defect sample the spectra have finite intensities at zero energy, which implies an occurrence of defect-induced intraband scattering [16,17].

The intensity of ERS was weak in the case of using the graphene on the Co substrate, especially for the SLG sample. Nevertheless, we managed to obtain such a spectrum (Fig. 6 and Fig. S3 in [30]) from the as-transferred flake. The line shape of this spectrum in the XY polarization geometry is similar to that measured on the Si/SiO$_2$ substrate, but the linear growth starts from ∼ 500–700 cm^{-1}. The energy of the G mode at the point of measurement was found to be 1581 cm^{-1}, and its reduced width of ∼10–11 cm^{-1} indicated the occurrence of doped carriers [31]. The detected intensity depletion at low frequencies (Fig. 6) implies the predicted threshold in the spectrum of the interband transitions due to a doping-induced shift of the Fermi level [16–20]. After the annealing of this sample at 200 °C during 7 h in an argon atmosphere, the
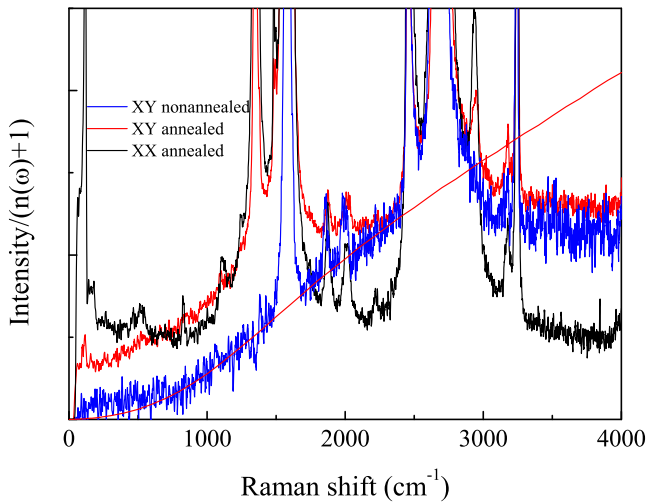
FIG. 6. (Color online) Electronic Raman spectra of SLG on Co substrate, measured at 300 K with linear polarizations using 532-nm excitation. Solid line presents the calculated spectrum for the case when the Fermi level is shifted by 60 meV from the Dirac energy.

frequency and width of the G band increased up to 1583 and 14–15 cm^{-1}, respectively, suggesting a decrease of carrier number (see the spectra in Fig. S3 in [30]). A blueshift of the 2D line from 2671 to 2689 cm^{-1} was found similarly to other publications [32]. Also, a strong increase of intensity of the disorder-induced D band at 1347 cm^{-1} was detected. The low-frequency behavior of the XY electronic continuum in such sample does not show any signatures of gap.

The enhancement of the D-mode intensity together with the emergence of some low-intensity phonon features in the XX spectra evidences an increased density of defects in the annealed sample, which provides a breakdown of the selection rules. As a result, the XX spectrum of the annealed sample demonstrates a surprising appearance of the narrow intense band at 117 cm^{-1} (see Fig. S3 in [30]). Its line shape is very asymmetric, showing the well-known Breit-Wigner-Fano (BWF) interference between the phonon and continuum [33]. This implies the appearance of the defect-induced low-energy electronic excitations, perhaps of the intraband type discussed in [16,17].

Thus for all investigated structures we observed the quasi-linear intensity increase in the low-frequency range of the spectra and the formation of the broad continua with maximum in the range of 0.3–0.4 eV. It should be noted that the continua line shapes and energy positions are somewhat different, both for different numbers of graphene layers and for different substrates used. One of the reasons for such a discrepancy may be interference effect in the case of the Si/SiO$_2$ substrate, which provides the dependence of the Raman intensity on the wavelength of the scattered light, though for the excitation energy used, 2.33 eV, this effect was found to be negligible [34]. The second reason may be an influence of the substrate itself, for example, charge-transfer effects in the case of the Co substrate. The found differences, however, do not change the general result. There is a broad continuum of the electronic excitations with a peak in the 0.3–0.4 eV range in all investigated structures on different substrates and without

substrate in the case of the bulk graphite. Similar results were obtained also in the measurements of freestanding multilayer graphene.

The experimental observation of the unambiguous A_{2g} symmetry of the interband electronic excitations in the ERS spectra of graphite and few-layer graphene on the cobalt substrate is consistent with the theoretical predictions [18–20] that indicate the conservation of the symmetry-conditioned pseudospin structure of the electron-hole pairs. On the other hand, the emergence of the intense electronic continuum in the XX polarization for the SLG and few-layer graphene on the Si/SiO$_2$ substrate and for annealed SLG on the Co substrate indicates the symmetry-breaking effect, which suggests an occurrence of channels of intervalley electron scattering. The higher intensity of the XX spectrum in a SLG sample with more defects suggests that defects also contribute to this effect. Thus the found manifestation of the symmetry-breaking effects shows that ERS is a rather sensitive tool for probing the broken-symmetry states of graphene structures.

A general feature of the graphite and few-layer graphene spectra is the observation of high-energy peaks near 0.8 eV. These bands are attributed to the transitions between the low-energy bands, degenerated in the Dirac point, and a pair of high-energy split bands. Near the K point of the BZ, these bands show the van Hove singularity, providing an evident contribution in the Raman spectra in comparison with the optical conductivity, which manifests only weak features observed at 0.7 and 0.9 eV [7]. The energies of the observed transitions are determined by the parameter of the interlayer interaction γ_1 in the Slonczewski-Weiss-McClure (SWM) model [35,36] of the graphite band structure, so the discovery of these transitions in the Raman spectra is useful for the refinement of the model parameters.

As we already mentioned, the emergence of the low-energy gap in the electronic Raman spectra is assumed based on recent ARPES data on the band structure of graphite [4]. The blocking of the low-energy transitions up to $2E_F$ was also predicted in the ERS spectra of doped graphene [16–20]. Such a depletion of the low-frequency intensity was detected in the cross-polarized XY ERS spectrum of the SLG as-transferred onto the cobalt substrate (Fig. 6). Together with the above-mentioned changes of the G-band phonon parameters, such a behavior verifies the occurrence of doped carriers and allows one to estimate the shift of the Fermi level from the charge neutrality point in $\sim$ 500 cm^{-1} (60 meV).

Uncovered in the Raman spectrum of the annealed SLG on the Co substrate, the low-energy band is attributed to the layer-breathing mode (LBM) with perpendicular displacement of the graphene layer, which is to some extent similar to the radial-breathing mode in single-walled carbon nanotubes [37]. Such a silent vibration has been observed in the range 80–120 cm^{-1} of Raman spectra of few-layer graphene [38,39], where it involves the relative displacement of the individual graphene layers in the vertical direction. The detection of the LBM is a challenge and its observation in the SLG spectra so far has not been reported on. The peak energy found, 117 cm^{-1}, is close to the LBM energies found for few-layer graphene and graphite (127 cm^{-1}) [40]. This indicates that the interaction between the graphene layer and the Co

substrate is comparable to the interlayer interaction in few-layer graphene.

The obtained experimental spectra were compared with the calculated from Eq. (1) spectra (divided by the Bose factor) in Figs. 1, 3, 5, and 6. The calculated Raman response in the graphite shows [solid lines in Figs. 1(a) and 1(b)] a rather good description of the low-energy experimental spectra, both at room and low temperatures. Following the ARPES data [4], the Fermi level in these calculations was placed by ~40 meV lower than the Dirac energy in the H point. The calculations of the response arising from transitions in the vicinity of the K and H points are presented in Fig. S4 in Ref. [30]. They evidence that the massive fermions near the K point in graphite provide a gradual linear increase of intensity from a finite value at zero energy in the low-temperature spectrum, while the excitations of massless fermions near the H point are blocked up to ~700 cm^{-1}. Nevertheless, the averaging of contributions from the low-energy transitions along the H-K line of the BZ, as in the case of optical conductance [7], results in the quasilinear intensity increase, in agreement with our low-temperature experimental results. The signs of the calculated threshold near ~700 cm^{-1} at the K point (see Fig. S4 in [30]) are still seen in the measured and calculated low-temperature spectra of graphite, but they are smeared by the temperature rise (Fig. 1). As a result, at 300 K the low-energy intensity growth in the calculated spectrum becomes flatter, which coincides with the experimental observations at room temperature (Fig. 1).

The calculated low-temperature Raman response for BLG is similar to the response from the K point in graphite and shows a linear increase from a finite intensity value at the low energies in the case when the Fermi level is placed in the charge neutrality point (Fig. S5 in [30]). The calculated spectra behavior transforms to the linear increase from zero intensity at $\omega = 0$ at room temperature (solid line in Figs. 3(a) and 3(b), and Fig. S5 in [30]), which corresponds to the experimental findings. Such spectral transformation is due to a variation of the Fermi factors with temperature. Thus a close agreement between the experimental and calculated data verifies the validity of the tight-binding model for the band structure of BLG. This result evidences a nonparabolicity of the low-energy bands near the K point of the BZ in BLG; the calculated spectrum behavior at 300 K in the case of parabolic zones is shown by the dashed line in Fig. 3(a). Such a behavior, as well as the energy-independent spectra behavior at low temperatures, was expected from the theoretical predictions based on a parabolic band dispersion in the vicinity of the K point in BLG [18–20]. The obtained discrepancy requires further investigations at different temperatures.

The room-temperature behavior of the calculated response of undoped SLG is rather different from that of the low-energy range (Fig. 5). A detailed check needs to be performed as to whether such a discrepancy is due to the Si/SiO$_2$ substrate effect and how it is connected to the discovered breaking of the scattering symmetry. In the case of SLG on the Co substrate, the response was calculated for the Fermi-level shift 60 meV to model carrier doping. The calculated spectrum (solid line in Fig. 6) describes the experimental data rather well, which confirms the carrier occurrence, which was indicated also by the variation of the G-band phonon parameters. The observed evolution of the spectra with doping verifies the theoretical predictions [16–20]; therefore the ERS spectra can be useful as an independent probe of the Fermi-level shift in doped graphene.

In all calculations performed, the high-energy behavior is dominated by the peak near 6 eV, as it was firstly shown in [16,17]. This result contradicts our observations and should be explained. One of the reasons for this discrepancy can be related to the decay of the electronic excitations due to the electron-electron and electron-phonon scattering [20]. However, the ARPES data in graphite [41] showed a rather small value (~50 meV) of the imaginary part of the electronic self-energy at a 1-eV shift from the Fermi level. A small effect of smearing was also observed for magnetoexcitons in the Raman experiments [25] even at room temperatures, which indicates a rather long lifetime of electronic excitations. Nevertheless, the reason for strong changes in the pseudospin structure at high energies, which determines the disappearance of the spin-flip scattering, should be cleared.

The energy dependence of the electron-photon vertex may also change the frequency behavior of the spectrum. Since it has not been theoretically predicted [20], another scattering mechanism has to be discussed. One such mechanism is based on an account of the intermediate states with the participation of phonons. Actually, the second-order resonant Raman scattering in graphitic systems [42–44] includes the strong phonon-assisted scattering of π and $\pi*$ electrons far (2–3 eV) from the Fermi level; however, similar processes, indeed, include states close to the Fermi level. It was shown [45] that in this case, the Feynman diagrams describing the two-phonon scattering also produce ERS. It is very possible that the observed electronic scattering in graphitic systems is due to such a phonon-assisted mechanism, which explains why the continua have the maximum in the range of multiphonon features but not at the energy of ~6 eV calculated from the band dispersion.

V. CONCLUSIONS

We present systematic research of the electronic Raman scattering in different graphitic structures. The continua of chiral electronic excitations with the energy of maxima ~0.35 eV were experimentally observed for all investigated samples. This is in contrast to theoretical estimation of the continua energy ~6 eV presented before [16,17]. The universal quasilinear behavior of the electronic continua was observed at low energies at room temperatures. The high-energy features first detected in graphite and few-layer graphene were attributed to the electronic transitions into (from) split $\pi*$ bands.

The influence of the substrate type and defect amount on the symmetry of electron-hole excitations was found. This suggests a modification of the pseudospin structure by external perturbations. The layer-breathing mode, silent in graphitic structures, was observed in the SLG spectrum.

Thus one can see that electronic Raman scattering at zero magnetic field is a sensitive tool for probing the low-energy electronic structure and pseudospin symmetry in pure and doped graphitic structures, and it has a potential for studying gapped structures formed by different methods.

[1] K. S. Novoselov, A. K. Geim, S. V. Morozov, D. Jiang, Y. Zhang, S. V. Dubonos, I. V. Grigorieva, and A. A. Firsov, Science **306**, 666 (2004).

[2] T. Ohta, A. Bostwick, T. Seyller, K. Horn, and E. Rotenberg, Science **313**, 951 (2006).

[3] T. Ohta, A. Bostwick, J. L. McChesney, T. Seyller, K. Horn, and E. Rotenberg, Phys. Rev. Lett. **98**, 206802 (2007).

[4] S. Y. Zhou, G.-H. Gweon, J. Graf, A. V. Fedorov, C. D. Spataru, R. D. Dieh, Y. Kopelevich, D.-H. Lee, S. G. Louie, and A. Lanzara, Nat. Phys. **2**, 595 (2006).

[5] K. F. Mak, M. Y. Sfeir, Y. Wu, C. H. Lui, J. A. Misewich, and T. F. Heinz, Phys. Rev. Lett. **101**, 196405 (2008).

[6] Z. Q. Li, E. A. Henriksen, Z. Jiang, Z. Hao, M. C. Martin, P. Kim, H. L. Stormer, and D. N. Basov, Phys. Rev. Lett. **102**, 037403 (2009).

[7] A. B. Kuzmenko, E. van Heumen, F. Carbone, and D. Van der Marel, Phys. Rev. Lett. **100**, 117401 (2008).

[8] Z. Q. Li, E. A. Henriksen, Z. Jiang, Z. Hao, M. C. Martin, P. Kim, H. L. Stormer, and D. N. Basov, Nat. Phys. **4**, 532 (2008).

[9] Y. Kopelevich, J. H. S. Torres, R. R. da Silva, F. Mrowka, H. Kempa, and P. Esquinazi, Phys. Rev. Lett. **90**, 156402 (2003).

[10] A. C. Ferrari, J. C. Meyer, V. Scardaci, C. Casiraghi, M. Lazzeri, F. Mauri, S. Piscanec, D. Jiang, K. S. Novoselov, S. Roth *et al.*, Phys. Rev. Lett. **97**, 187401 (2006).

[11] P.-H. Tan, S. Dimovski, and Y. Gogotsi, Philos. Trans. R. Soc., A **362**, 2289 (2004).

[12] A. A. Abrikosov and L. A. Fal'kovskii, Zh. Eksp. Teor. Fiz. **40**, 262 (1961) [Sov. Phys. JETP **13**, 179 (1961)].

[13] B. Kh. Bairamov, V. A. Voitenko, and I. P. Ipatova, Uspekhi Fizicheskikh Nauk **163**, 67 (1993); Sov. Phys.-Usp. **36**, 392 (1993).

[14] T. P. Devereaux and R. Hackl, Rev. Mod. Phys. **79**, 175 (2007).

[15] Yu. S. Ponosov and S. V. Streltsov, Phys. Rev. B **86**, 045138 (2012).

[16] H.-Y. Lu and Q.-H. Wang, Chin. Phys. Lett. **25**, 3746 (2008).

[17] H.-Y. Lu, S. Chen, Y. Xu, L.-Q. Zhang, D. Wang, and W.-S. Wang, Phys. Rev. B **88**, 085416 (2013).

[18] O. Kashuba and V. I. Fal'ko, Phys. Rev. B **80**, 241404 (2009).

[19] M. Mucha-Kruczynski, O. Kashuba, and V. I. Fal'ko, Phys. Rev. B **82**, 045405 (2010).

[20] O. Kashuba and V. I. Falko, New J. Phys. **14**, 105016 (2012).

[21] C. Faugeras, M. Amado, P. Kossacki, M. Orlita, M. Kühne, A. A. L. Nicolet, Yu. I. Latyshev and M. Potemski, Phys. Rev. Lett. **107**, 036807 (2011).

[22] M. C. Kuhne, C. Faugeras, P. Kossacki, A. A. L. Nicolet, M. Orlita, Yu. I. Latyshev, and M. Potemski, Phys. Rev. B **85**, 195406 (2012).

[23] P. Kossacki, C. Faugeras, M. Kuhne, M. Orlita, A. A. L. Nicolet, J. M. Schneider, D. M. Basko, Yu. I. Latyshev, and M. Potemski, Phys. Rev. B **84**, 235138 (2011).

[24] Y. Kim, Y. Ma, A. Imambekov, N. G. Kalugin, A. Lombardo, A. C. Ferrari, J. Kono, and D. Smirnov, Phys. Rev. B **85**, 121403 (2012).

[25] Y. Ma, Y. Kim, N. G. Kalugin, A. Lombardo, A. C. Ferrari, J. Kono, A. Imambekov, and D. Smirnov, Phys. Rev. B **89**, 121402 (2014).

[26] A. F. Garcia-Flores, H. Terashita, E. Granado, and Y. Kopelevich, Phys. Rev. B **79**, 113105 (2009).

[27] B. Partoens and F. M. Peeters, Phys. Rev. B **74**, 075404 (2006).

[28] D. D. L. Chung, J. Mater. Sci. **37**, 1475 (2002).

[29] T. A. Nguyen, J.-U. Lee, D. Yoon, and H. Cheong, Sci. Rep. **4**, 4630 (2014).

[30] See Supplemental Material at http://link.aps.org/supplemental/10.1103/PhysRevB.91.195435 for details concerning graphene samples characterization, the ERS spectra measurements, and calculations.

[31] Jun Yan, Yuanbo Zhang, Philip Kim, and Aron Pinczuk, Phys. Rev. Lett. **98**, 166802 (2007)

[32] Z. H. Ni, Z. M. Wang, Z. Q. Luo, Y. Y. Wang, T. Yu, Y. H. Wu, and Z. X. Shen, J. Raman Spectrosc. **41**, 479 (2010).

[33] M. V. Klein, *Light Scattering in Solids I*, edited by M. Cardona (Springer-Verlag, Berlin, 1983), pp. 147–202.

[34] Duhee Yoon, Hyerim Moon, Young-Woo Son, Jin Sik Choi, Bae Ho Park, Young Hun Cha, Young Dong Kim, and Hyeonsik Cheong, Phys. Rev. B **80**, 125422 (2009).

[35] J. C. Slonczewski and P. R. Weiss, Phys. Rev. **109**, 272 (1958).

[36] J. W. McClure, Phys. Rev. **104**, 666 (1956).

[37] A. M. Rao, E. Richter, S. Bandow, B. Chase, P. C. Eklund, K. A. Williams, S. Fang, K. R. Subbaswamy, M. Menon, A. Thess, R. E. Smalley, G. Dresselhaus, and M. S. Dresselhaus, Science **275**, 187 (1997).

[38] Jingzhi Shang, Chunxiao Cong, Jun Zhang, Qihua Xiong, Gagik G. Gurzadyana, and Ting Yua, J. Raman Spectrosc. **44**, 70 (2013)

[39] Chun Hung Lui, Zhipeng Ye, Courtney Keiser, Xun Xiao, and Rui He, Nano Lett. **14**, 4615 (2014).

[40] R. Nicklow, N. Wakabayashi, and H. G. Smith, Phys. Rev. B **5**, 4951 (1972).

[41] C. S. Leem, B. J. Kim, C. Kim, S. R. Park, T. Ohta, A. Bostwick, E. Rotenberg, H.-D. Kim, M. K. Kim, H. J. Choi, and C. Kim, Phys. Rev. Lett. **100**, 016802 (2008).

[42] C. Thomsen and S. Reich, Phys. Rev. Lett **85**, 5214 (2000).

[43] J. Maultzsch, S. Reich, and C. Thomsen, Phys. Rev. B **70**, 155403 (2004).

[44] A. C. Ferrari and D. M. Basko, Nat. Nanotechnol. **8**, 235 (2013).

[45] M. V. Klein, Phys. Rev. B **24**, 4208 (1981).